








Cite this: *J. Anal. At. Spectrom.*, 2017, **32**, 2182

Improved detection sensitivity for heavy trace elements using a miniature laser ablation ionisation mass spectrometer

R. Wiesendanger, ^{ac} M. Tulej, ^a A. Riedo, ^{ab} S. Frey,^a H. Shea ^c and P. Wurz ^a

Laser ablation ionisation time-of-flight mass spectrometry is a versatile technique to obtain highly sensitive measurement of the elements and isotope composition of solid materials. Because of the measurements of nearly all elements in the sample, large ion rates of abundant elements may reduce the detection efficiency for heavier elements arriving later at the detector system. If this occurs, it will affect the capability of quantitative measurements of heavy species. We demonstrate that by implementation of a short high-voltage (HV) pulse, we can remove the high rate ions that reduce the detection efficiency of the ion detector to measure trace elements, which otherwise would not be detectable. The location of a suitable electrode in the given ion optical system, the timing and the pulse shape were determined with the help of numerical ion trajectory simulations using the SIMION software. An HV pulse removes ions of lighter elements, including Na, K, and Mg from the analysed ion beam, which are typically the most abundant species in rocks and soils, allowing sensitive analysis of heavy trace elements. Using standard NIST reference materials we determined detection limits in the sub-ppm range and accomplished isotope ratio measurements of Pb with an accuracy in the per mill range. Further investigations of trace elements of the KREEP material in a lunar sample demonstrate that the miniature LIMS system can be used for *in situ* analysis of rocks and soils, and for investigations of geological processes and dating.

Received 23rd May 2017
Accepted 21st August 2017

DOI: 10.1039/c7ja00193b

rsc.li/jaas

Introduction

Laser ablation ionisation time-of-flight (LIMS-TOF) mass spectrometry is a well-known laboratory technique for a direct measurement of the chemical composition of solid materials.^{1–7} First commercial instruments were used widely in the 1980s and 1990s (*e.g.*, LAMMA and LIMA 2A).⁸ Nevertheless, due to difficulties in controlling the laser ablation ion source conditions and a poor mass resolution, the number of applications of this technique decreased in the early years of our century, mainly due to its semi-quantitative performance. At that time, possible improvements to this method were considered⁹ and different miniature laser ablation ionisation mass spectrometers (with instrument names LASMA,^{10–12} LAMS,¹³ and LMS¹⁴) were developed for space research. To comply with the severe mass, volume and power constraints on board a spacecraft, a lander platform or a rover,¹⁴ these TOF analyzers have drift lengths of typically 20–30 cm, some are even shorter.¹⁵ The

limited size of the mass analyser implies challenges, particularly in terms of mass resolving power. However, progress in material science and technology, laser technology, electronics, ion detection and data acquisition systems, and improvements of modelling tools and computing capabilities have opened new perspectives for this technique, including the miniature instruments designed for space research. Currently, highly sensitive analysis of solid materials using a laser ablation ion source and time-of-flight technique was reported by several groups.^{3,4,6,13,16–20} Many drawbacks of early LIMS systems, including the low stability of the ion source, low mass resolution and semi-quantitative performance were overcome by using UV and short-pulse laser ablation ion sources.^{6,21–23}

LIMS instruments can be used to record the chemical composition of any solid material with high spatial and depth resolutions (down to the nanometre scale),¹⁸ which is of considerable interest to various applications.^{3,16–18} In particular, by increasing the sensitivity and accuracy of the quantitative element and isotope analysis, the LIMS instruments can be valuable in investigations of planetary surfaces yielding mineralogical, elemental and isotope composition of rocks and soils.^{1,5,24} Especially highly sensitive analysis of minor and trace elements and their isotopes would be of high scientific interest to investigate geological formation processes, perform material dating, and record biomarkers of extinct or extant life on other

^aSpace Research and Planetary Sciences, Physics Institute, University of Bern, Switzerland

^bSackler Laboratory for Astrophysics, Leiden Observatory, Leiden University, The Netherlands

^cMicrosystems for Space Technologies Laboratory, Ecole Polytechnique Fédérale Lausanne, Switzerland

planetary bodies in our solar system. Our current laser ablation ion source delivers an intense beam of ions and the TOF analyser has high ion transmission because of its grid-less design. Because of the small size of the mass analyser, saturation of the ion detector can reduce the instrument's performance. Typically, a multi-channel plate (MCP) ion detector system has a large dynamic range, and thus it is also highly sensitive.²⁵ However, when ion rates exceed values of about $10^7/\text{sec}$,²⁶ the detector becomes saturated and for a certain time, its sensitivity can be significantly reduced due to the dead time of triggered microchannel pores (recovery time of hundreds of nanoseconds to milliseconds).²⁷ For TOF mass spectrometers, this means that elements arriving later on at the detector system will be measured with lower sensitivity or not detected at all because less active MCP pores are available.

In this contribution, we report on the improvements to ion detection by implementing a short-pulse high-voltage (HV) switch (called "pulser" later on in this publication) designed to eliminate low-mass ions. This improves the detection sensitivity for heavier mass elements, because a larger proportion of the detector area is still 'fresh' upon their arrival. This method can be of considerable interest when the sample (typically a rock sample) has large concentrations of light elements ($m < 40$ u), such as C, O, Na, Mg, and K, and small concentrations of heavy elements ($m > 60$ u), such as Sr, Rb, Mo, Ba, Pb, Th and U. To suppress the ions of the abundant elements before they arrive at the detector system in the TOF mass spectrometer, the pulser switches between two voltage sets. One set transmits ions to the detector, and one set rejects them. This approach has been successfully implemented in other instruments.^{28,29} In our compact LIMS system (with instrument name LMS) with a given mechanical and ion-optical design, there is no space for the integration of an additional electrode. Thus, one of the existing electrodes in the ion optical system had to be selected to perform ion rejection. The electrode selection was based on extensive ion-optical modelling and ion trajectory simulations. The modelling showed that the selected electrode for the pulser application allows effective rejection of major light elements without noticeably affecting ion distribution of heavier elements.

Experimental

Theory and simulation

The ion trajectory analysis was performed using the SIMION (Scientific Instrument Services, Inc.) software (Windows7, 64 bit, 2.8 GHz Intel Core i7 2600S, 32 GB DDR3 DIMM 1333 MHz RAM). In the modelling studies, the initial ion cloud contained 314 040 particles representing the elements and isotopes with their abundances as quoted for the National Institute of Standards and Technology (NIST) 664 reference material. One exception is the main element iron, whose abundance had to be reduced by a factor of 1000 to decrease computing time to 15 min per run. The modelling provides the pulse shape, timing and the location at which the HV pulse shall be applied. One of the existing electrodes in the ion optical system was found to be suitable for the application of the pulse.

To perform optimal ion rejection of unwanted ions by the pulser, a sufficiently long delay between light and heavy masses of interest should be maintained (~ 100 ns). Under these conditions, the applied HV voltage pulse can switch between a "rejecting" and a "transmitting" voltage, without significantly affecting the ion population of heavier masses. Fig. 1 displays a simulated TOF spectrum at the electrode defined for the pulser. The solid curves represent the individual approximated temporal distribution of particular ion species abundant in the simulated NIST 664 reference material while passing through the aperture of the repelling electrode (Gaussian envelopes).

The grey envelopes are the sum of all species in the beam. One can observe one group of three species, (Ta, W, and Pb) that is delayed by more than 250 ns from the main element iron and by 100 ns from Mo. This analysis indicates that the selection of these heavy elements can be performed by rejecting groups of lighter elements. In the present study, we focus just on the group containing the Ta, W and Pb elements. All elements up to and including Mo should be removed from the beam. The ion trajectory simulation indicates that this can be achieved by applying the repulsive voltage for 550 ns after the moment of ion formation (the moment of laser ablation taken as $t = 0$). After this period of time, the voltage is switched to the transmitting set. This removes all ions with mass/charge < 96 u/e, while Ta, W and Pb will be transmitted to the detector system without losses. A choice of a pulse with +500 V (ion rejection) and -1550 V (ion transmission) is found to be optimal for effective ion rejection or transmission, respectively. Furthermore, a positive rejection potential was chosen to prevent ions from further entering into the TOF analyser. By applying this HV pulse, the ions are sent backwards onto the electrodes or the instrument walls, while the subsequently applied negative potential at this electrode is used to efficiently transmit the ions of interest towards the detector.

Instrument setup, material and methods

Our miniature LIMS system is a grid-less reflectron-type TOF mass spectrometer of cylindrical symmetry. The details of the experimental setup and principles of operation of LMS can be

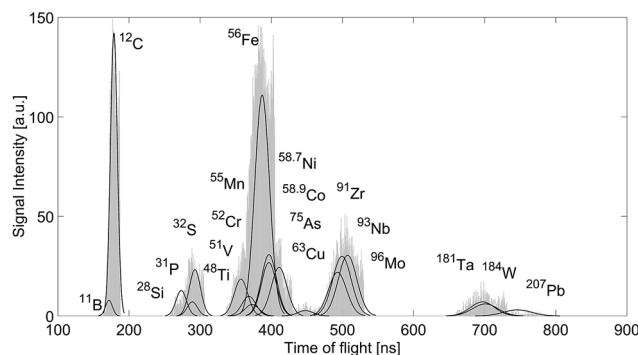


Fig. 1 Simulated time-of-flight spectrum at the pulsed electrode. The histogram shows the intensity of the ion flux assuming the NIST 664 reference material. The solid lines are fitted gauss curves for each individual element.

found in our previous publications.^{1,4,14} In the current setup, a HV pulser is introduced to change the potential of an electrode in the ion optical system and its operation is incorporated into the measurement cycle. A simplified schematic drawing of the LMS instrument and the principle of operation are shown in Fig. 2. The ion source combines a pulsed laser system ($\lambda = 775$ nm, $\tau \sim 190$ fs, repetition rate ≤ 1 kHz, intensity ≤ 1 mJ per pulse) with an optical system capable of focusing the laser beam to a spot size of about $\varnothing 10\text{--}15$ μm on the sample surface. The investigated samples are positioned about a fraction of mm away from the entrance into the mass analyser and can be moved by a xyz-micro-translation stage. Only positively charged ions that are produced during the laser ablation/ionization process can enter the ion optical system of LMS where they are subsequently accelerated, confined and focussed into a field-free drift tube. While travelling towards the detector system, the ions pass the field free space and are reflected and time-focused on the detector entrance plane by the ion mirror (reflectron). After passing again through the field free space, they arrive at the MCP detector system. The MCP detector system is a multi-readout system allowing measurements with a high dynamic range of about 10^8 and with sensitive detection of elements down to sub ppm levels.^{20,30} In the current setup, two high speed ADC cards (8 bit, 2 channels each, sampling speed up to 4 GS s^{-1}) are used to record the electrical signals generated by the MCP detector system. The laser system, the micro-translation stage and the data acquisition system are controlled remotely by a custom-made software.⁴ If required, performance optimization software is used to control the ion optical settings and obtain the optimal operation conditions of the instrument in terms of ion transmission and mass resolution.³¹ The optimizer software can also be used with a pulser introduced in the measurement loop.

The high-voltage pulser used in this study is based on a Behlke FSWP 51-02 high-speed switch (with about 10 ns rise and fall time)³² with a custom made floating ground and two HV inputs enabling operation across the electrical ground, from a positive to a negative voltage. The positive voltage is necessary to efficiently repel the positively charged ions with energies exceeding several hundreds of electron volts from the laser ablation process.³³ The negative voltage is needed for focussing the ions on the detector. The electronic box of the pulser is located outside the vacuum chamber and the generated HV pulse is routed to the pulsed electrode through dedicated, impedance matched shielded cable. An appropriate matching of the impedance was found necessary to minimise the settling time of the pulsed electrode and thereby excludes influence on the heavy elements under investigation.

A wiring scheme with HV pulse implementation is shown in Fig. 2. The laser control unit generates a trigger signal for each laser pulse, which initiates the two data acquisition cards⁴ and a second delay generator (DG645, Stanford Research) that is used to generate the variable time delay for the pulser.

We used the NIST 664 reference material for the determination of the detection limits and the demonstration that Pb at a trace element concentration of 240 ppm weight fraction (wf), (corresponding to a 63 ppm atomic fraction (af)) can be

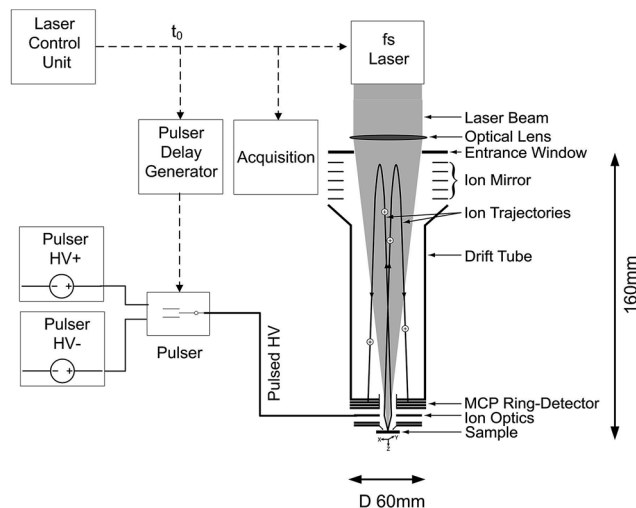


Fig. 2 Construction scheme of the LMS instrument. The ions produced in the laser ablation/ionisation source enter into the instrument through the small circular aperture and are subsequently confined and accelerated into the instrument using the source ion optical system. The ion mirror reflects and focusses the ions on the detector. One of the source electrodes is used to enable pulser operation.

detected. The NIST SRM 981 common lead isotope standard material is used to study the isotope composition of Pb and for testing if the usage of the pulser affects the measured Pb isotope abundance. Finally, measurements on a Sayh al Uhaymir 169 lunar meteoritic sample were conducted to demonstrate the performance of the instrument in measurements of natural samples.^{27–29}

The measurements of the mass spectra were conducted by accumulation of several thousands of individual single laser shot mass spectra. This method increases the signal-to-noise ratio (SNR) to yield well-averaged measurements with good statistics. The TOF spectra are scaled to a mass scale using the simple transformation equation $m = a(t + b)^2$, where m is the mass in unified atomic mass units [u], t is the measured time of flight, and a and b are the calibration constants.²⁰ Typically, the mass calibration accuracy of about 500 ppm is achieved for mass spectra with a mass resolution ($m/\Delta m$) in the range 500–600.²⁰ For the quantitative analysis, peak areas are obtained by direct integration of the measured signals,³⁴ from which atomic fractions (af) for each species are derived, and which are further converted to weight percent (wf) for comparing the measurements results and quoted NIST values.

Results and discussion

Performance evaluation using NIST standards

A typical mass spectrum measured for the NIST 664 sample and the peak intensities expected from the element abundance quoted by the NIST are shown in Fig. 3 by red bars (accumulation of 1000 single laser shot mass spectra).

For elements lighter than ⁵⁶Fe, we observe good agreement with the measured peak intensities. Some discrepancies

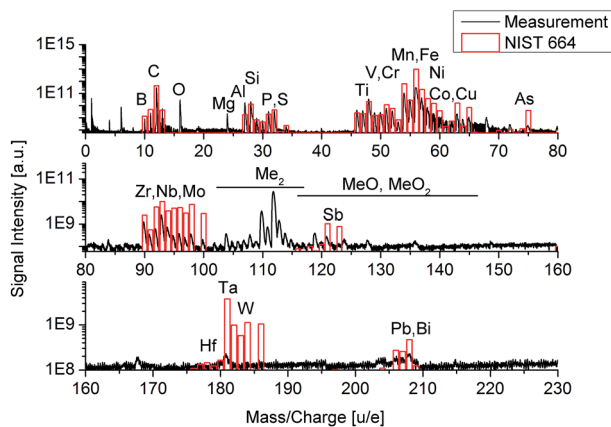


Fig. 3 The mass spectrum (line spectrum) of the NIST664 sample and the quoted peak intensities (bars) derived from the reference data document without the pulser.

between the quoted and measured peak intensities for Mg and Al mass peaks are attributed to the contribution from the carbon clusters (*e.g.*, C₂ and C₂H₃). In addition, the ⁵⁶Fe mass peak is likely to be recorded at detector saturation because of the high concentration of Fe in the NIST 664 sample (96.7% wf/94.1% af). The measurements of other elements are close to the quoted values. Also for these elements, their relative sensitivity coefficients (RSCs) are close to one, as has been reported previously.⁴ For the elements heavier than Fe, the peak intensities are observed to decrease systematically with increasing mass, sometimes to a dramatic extent. The intensities for Cu, Mo, Ta and W are observed to be about a factor of ten lower than expected. This is mostly due to large ion rates of the Fe ions on the detector causing a dramatic decrease in the detection efficiency for the heavier ions, together with a reduced spectral quality (asymmetric peak shape, disturbed background line) of heavier elements than Mo.

Hence, after removing high abundance ions from the ion beam (masses lighter than Mo), an increase of the intensities of the peaks of heavy trace elements including Ta, W and Pb is expected.

Determination of detection limits and isotope accuracy with the pulser

Fig. 4a shows the measurement of the Ta–W–Hf group of elements obtained by the accumulation of 100 000 single laser shot mass spectra while low-mass ions are eliminated by the pulser. These spectra were used to determine the detection limits and the mass peaks of the isotopes ¹⁸¹Ta, ¹⁸³W and ¹⁸⁶W were selected for further quantitative analysis because they are free of major isobaric interferences and are measured with a high SNR. All mentioned isotopes have a certified abundance of more than 140 ppm wf, which corresponds to about 40 ppm af. The terrestrial abundances of the isotopes were assumed in this estimation.³⁵ From the SNR of the detected peaks, the detection limits down to 8–14 ppm wf (2–4 ppm af) were derived and the determined limits are summarized in Table 1. The mass peaks of Hf are also observed in the spectrum and their SNRs indicate that the Hf is measured at the determined detection limit.

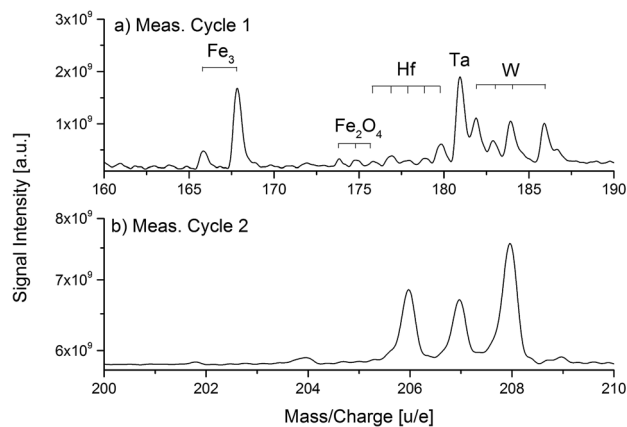


Fig. 4 Mass spectrum in the range of 160–190 m/q and the mass spectrum of Pb and Bi taken with pulser.

However, the presence of Fe metal clusters makes this identification less certain. Fig. 4b shows the mass spectrum of Pb obtained from the NIST 664 while low-mass ions are eliminated by the pulser (accumulation of 20 000 single laser shot mass spectra). The determined detection limits are also reported in Table 1.

These studies showed that for the lowest laser fluences where lead mass peaks could be observed, no other elements could be measured because the ablation threshold for lead is significantly lower than those for other elements, including Ta and W. At the applied laser fluences, relative sensitivity coefficients are also observed to be sensitive to the applied laser fluences. The quantitative analysis of the element abundances were performed for the largest applied laser fluences, for which it is expected that the sensitivity coefficients are close to each other for the measured elements. From this analysis, the detection limits for lead are derived to be at 1 ppm per wf (200–300 ppb per af). Also, the element Bi is readily observed in the spectrum at a S/N ratio of 6. Its abundance is determined at 9 ppm per wf (2.3 ppm per af), which is found to be consistent with the values determined previously.^{1,20}

The influence of the pulser on the Pb isotope composition was investigated using the NIST SRM 981 isotope standard sample. The measurements were performed in the laser fluence range between 60 nJ cm⁻² and 1 μJ cm⁻². Correlated with higher

Table 1 Abundance and calculated detection limits for selected isotopes for measurements with the pulser

Element	Isotope	SNR	Certified abundance [ppm per wf]	Detection limit [ppm per wf]	
Ta	181	80.5	1099.9	13.7	
	W	183	13.5	143.1	10.6
		186	34.7	284.3	8.2
Pb	204	6.9	3.4	0.5	
	206	68	57.8	0.9	
	207	56.1	53.0	0.9	
	208	122.9	125.8	1.0	
Bi	209	6.3	9	1.4	

fluences, a peak broadening is observed and attributed to space charge effects due to the large ion concentration. At lower laser fluences a smaller width of the Pb mass peaks was obtained and hence also a better mass resolution.

The results from the measurements with and without applying the pulser were compared. They are statistically well-averaged and consist of 77 000 and 56 000 single laser shot mass spectra, respectively (Fig. 5a and b). For both measurements, the resolution and SNR of the ^{208}Pb isotope are larger than 550 and 220, respectively. The determined isotopic ratios and their relative accuracies are shown in Fig. 5c. The relative isotope ratio accuracies were calculated according to the following expression:

$$\text{Acc}_{\text{rel}} = \frac{|\text{Abundance}_{\text{Meas}} - \text{Abundance}_{\text{Ref}}|}{\text{Abundance}_{\text{Ref}}}$$

The values for the isotope abundances for the measurements with and without applying the pulser agree within the experimental uncertainty (Fig. 5c). The pulser seems not to have an effect on the isotope abundance at the accuracy level of the current experiment. Due to the overall quality of the recorded spectra (baseline shape, noise levels), the accuracy is not optimal and expected to improve with optimized instrument parameters.

Studies of trace elements in a lunar meteorite

LIMS measurements on the Sayh al Uhaymir 169 lunar meteorite were conducted by applying the pulser to repel low mass ions and hence to improve the detection sensitivity for heavier elements. The meteorite sample was well-studied so far using a number of other analytical techniques including inductively

coupled mass spectrometry and optical emission spectrometry.^{36–38}

The sample contains impact melt breccia with zircon grains of high content of trace elements with concentrations at ppm/wf levels. The current measurements were conducted on zircon grains, known to be typically highly abundant in Pb, Th and U. These three elements are also the key elements for radioisotope geochronology. However, such studies can be challenging for miniature mass spectrometers. The major elements in the mineral are of relatively low mass compared to the trace elements of interest, and the detector saturation maybe unavoidable. The low mass elements, on the other hand, have a sufficiently large time separation compared to the heavy elements Pb, Th, or U at the location of the pulsed electrode and the pulser can likely be used successfully in these studies.

Fig. 6a shows the higher mass/charge section of a typical mass spectrum of a zircon grain (accumulation of 19 800 single laser shot mass spectra). All zirconium isotopes and their oxides are readily visible, and the light trace element ^{89}Y can also be observed. As expected, no trace elements with masses larger than 90 u were found in the spectrum. This was expected due to detector saturation caused by the high rate of zirconium ions.

Thus, by applying the pulser for removing the Zr ions from the beam, one would expect an improvement of the measurement sensitivity to the heavier elements. Fig. 6b confirms this expected signal recovery. It shows the SNR of the dominant groups shown in Fig. 6a compared to the trace element SNR. The data have been obtained by tuning the pulser timing, while keeping all other instrument parameters constant. A short delay corresponds directly to a low cut-off mass and an increasing delay time means that more heavy species are removed from the beam as explained in the theoretical section and illustrated in Fig. 1. The SNR of the analysed mass peaks were obtained by using peak area integration after background line subtraction.

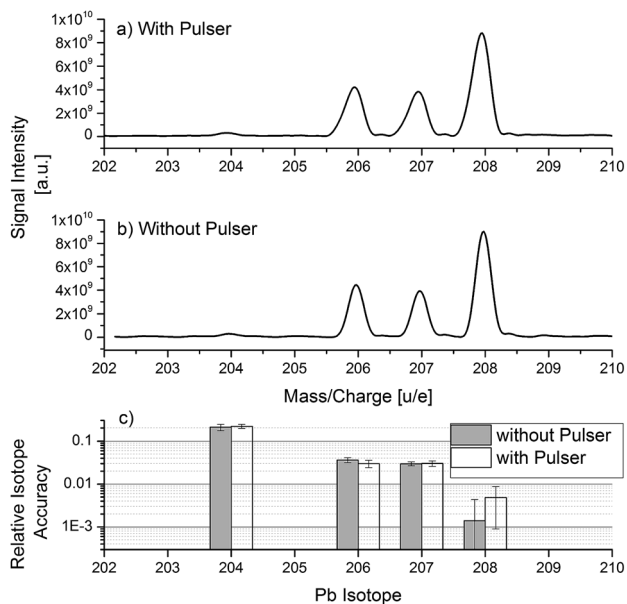


Fig. 5 Comparison of Pb spectra with (panel a) and without the pulser (panel b) on the NIST SRM 981 isotope standard. The isotope ratios are determined to be similar within the experimental accuracies (panel c).

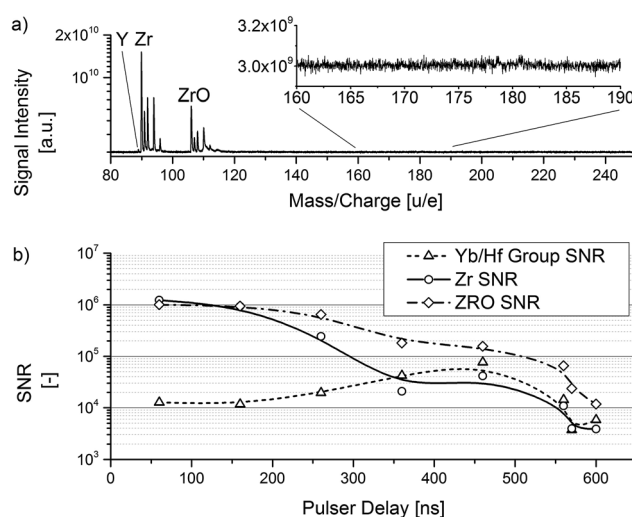


Fig. 6 (a) High-mass part of a spectrum taken on a Zr grain on the Sayh al Uhaymir meteorite. Saturation of the detector prevents detection of heavy trace elements with $m/q > \sim 120$. (b) Desaturation of the MCP detector and increase of trace element signal strength.

The noise level was determined as the standard deviation of the measured curve in a portion of the spectra where no other signals except the baseline were present.³⁴ Although mass resolutions larger than 300 were achieved on Hf, it was not possible to completely resolve individual peaks in the mass spectrum, especially for the readily saturated Zr. Thus, the overall groups of isotopes and clusters were integrated to investigate the variation of the signal intensities. The first group contained all Zr isotopes from 90–96 u/e and the second group all Zr oxides (106–112 u/e). The third group contained all isotope mass peaks in the mass range between 186 and 180 u/e, corresponding mainly to Yb, Tm, Lu and Hf, as representatives of trace elements. The spectra were taken at six different pulser delays (60 ns, 160 ns, 260 ns, 360 ns, 460 ns, 560 ns, and 600 ns). Each of the spectra was composed of 10×100 individual single laser shot mass spectra. The relatively high values of the calculated SNR results from the signal intensity were calculated for a whole group of peaks, but not for the individual peaks. This leads to a relatively high value for the integrated area and therefore to a larger SNR.

The Zr and ZrO signals at short pulser delays as shown in Fig. 6b are saturated, which is expressed by the flat section up until about 200 ns. Within this section, the Hf/Yb group SNR is around 10^4 .

With increasing pulser delay, the mass peak intensities of Zr decrease gradually. The ZrO intensity also decreases with an approximately constant time offset of about 100 ns with respect to Zr. Correlated to the decrease of the Zr and ZrO signal, an increase of the SNR of the trace element group is observed. The SNR reaches a plateau of 5×10^4 at a 450 ns delay. Any further increase of the pulser delay will decrease the signal intensity of the trace element group because the pulser cut-off time also starts to affect this group. Finally, all signal intensities drop down when the repelling pulse suppresses all ions from the beam. Note that the curve of the Zr and Yb is flat in the region of its maximum, which indicates that a precise timing of the pulser application is not required to obtain optimal mass peak intensities for the heavier elements. The pulser delays found in the current experiment agree well with the delay determined in the ion-optical simulations shown in the first section.

Fig. 7 shows a mass spectrum of the trace elements measured after applying the pulser under optimal timing conditions (accumulation of 79 500 single laser shot mass spectra). A series of the heavier lanthanides, including Dy, Ho, Er, Th, Yb and Lu, and the transition metal group, including Hf and the major peaks of W at 184 and 186 u/e are measured.

Although Pb is generally easy to ionize and should be observed at the abundance levels given in the literature,³⁹ it was not detected in the selected sample region. Thus, we conclude that the Pb concentration was below the detection limit in the investigated zircon inclusion. Nevertheless, the Th and U elements and their oxides were readily detected with the LMS instrument. In this measurement an average Th/U ratio of 0.44 ± 0.08 was measured, while a ratio of 3.8 is determined from the reference study of this sample.³⁹ We identified two main reasons for this difference:

First, the concentrations in the reference study represent the results of a bulk analysis performed on powder aliquots, while

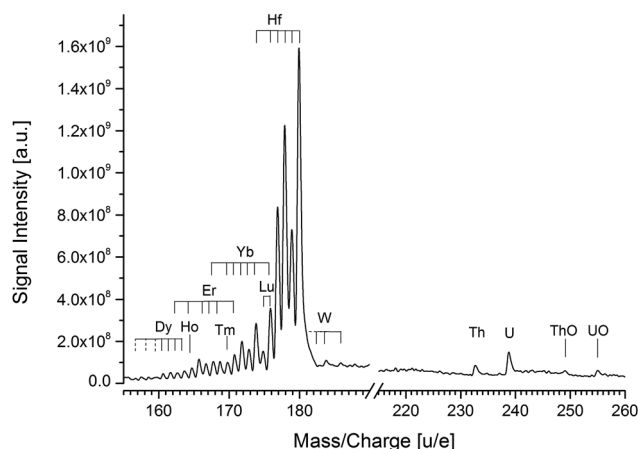


Fig. 7 High-mass part of a mass spectrum of the KREEP sample. The trace elements can be easily observed.

our measurement represents a microanalysis on a $\sim 15 \mu\text{m}$ sized spot. Averaging of the concentrations over many spots on this sample could lead to values that are more comparable.

Second, due to missing RSCs for heavy elements, the presented values are determined from uncorrected raw data. An extension of the RSC catalogue to heavy elements like Th and U would be a future step to quantification and accurate isotope measurements allowing dating of the lunar meteorite.

Conclusions

In the present study, we showed that elements of high abundance reduce the detector sensitivity for the subsequent mass peaks in a mass spectrum in a time-of-flight instrument. Removing such elements from the spectrum is a way to reduce detector saturation effects and increase sensitivity to elements of interest at higher mass. We showed by the simulations performed with SIMION that this technique can be implemented in our miniature LIMS system using a fast high voltage switch (pulser) applied to an existing electrode of the ion-optical system. The pulser allows extending the measurement capabilities of the instrument to heavy trace elements with concentrations in the low ppm (weight fraction) range. We improved the detection limits for heavy trace elements using the pulser on a NIST 664 standard material and showed that the accuracy of the measured isotope ratios is not affected by the pulser operation on the NIST 981 lead isotope standard. This is especially of high interest in the context of radioisotope dating of solids using the elements Pb and U, because it allows dating with an improved accuracy.

We successfully applied the pulser technique to the Sayh al Uhaymir 169 lunar meteorite to record heavy trace elements up to U and its oxides, which have not been detected so far with our instrument.

Conflicts of interest

There are no conflicts of interest to declare.

Acknowledgements

This work is supported by the Swiss National Science Foundation. We are grateful for the help by Jürg Jost, Roland Nussbaum, Christoph Josi from the electronics workshop. We thank B. Hofmann of Naturhistorisches Museum der Burgergemeinde Bern for kindly providing us with the SAU 169 lunar sample.

Notes and references

- 1 A. Riedo, S. Meyer, B. Heredia, M. B. Neuland, A. Bieler, M. Tulej, I. Leya, M. Iakovleva, K. Mezger and P. Wurz, *Planet. Space Sci.*, 2013, **87**, 1–13.
- 2 V. Grimaudo, P. Moreno-Garcia, A. Riedo, S. Meyer, M. Tulej, M. B. Neuland, M. Mohos, C. Gutz, S. R. Waldvogek, P. Wurz and P. Broekmann, *Anal. Chem.*, 2017, **89**, 1632–1641.
- 3 M. Tulej, A. Neubeck, M. Ivarsson, A. Riedo, M. B. Neuland, S. Meyer and P. Wurz, *Astrobiology*, 2015, **15**, 669–682.
- 4 A. Riedo, M. Neuland, S. Meyer, M. Tulej and P. Wurz, *J. Anal. At. Spectrom.*, 2013, **28**, 1256–1269.
- 5 M. B. Neuland, S. Meyer, K. Mezger, A. Riedo, M. Tulej and P. Wurz, *Planet. Space Sci.*, 2014, **101**, 196–209.
- 6 B. C. Zhang, M. H. He, W. Hang and B. L. Huang, *Anal. Chem.*, 2013, **85**, 4507–4511.
- 7 M. He, Y. Meng, S. Yan, W. Hang, W. Zhou and B. Huang, *Anal. Chem.*, 2017, **89**, 565–570.
- 8 M. J. Southon, M. C. Witt, A. Harris, E. R. Wallach and J. Myatt, *Vacuum*, 1984, **34**, 903–909.
- 9 A. A. Sysoev and A. A. Sysoev, *Eur. J. Mass Spectrom.*, 2002, **8**, 213–232.
- 10 G. G. Managadze, P. Wurz, R. Z. Sagdeev, A. E. Chumikov, M. Tuley, M. Yakovleva, N. G. Managadze and A. L. Bondarenko, *Sol. Syst. Res.*, 2010, **44**, 376–384.
- 11 L. M. Zelenyi and A. V. Zakharov, *Sol. Syst. Res.*, 2010, **44**, 359–361.
- 12 L. M. Zelenyi, A. V. Zakharov, G. M. Polischuk and M. B. Martynov, *Sol. Syst. Res.*, 2010, **44**, 15–25.
- 13 W. B. Brinckerhoff, G. G. Managadze, R. W. McEntire, A. F. Cheng and W. J. Green, *Rev. Sci. Instrum.*, 2000, **71**, 536–545.
- 14 U. Rohner, J. A. Whitby and P. Wurz, *Meas. Sci. Technol.*, 2003, **14**, 2159–2164.
- 15 U. Rohner, J. A. Whitby, P. Wurz and S. Barabash, *Rev. Sci. Instrum.*, 2004, **75**, 1314–1322.
- 16 A. Riedo, V. Grimaudo, P. Moreno-Garcia, M. B. Neuland, M. Tulej, P. Wurz and P. Broekmann, *J. Anal. At. Spectrom.*, 2015, **30**, 2371–2374.
- 17 V. Grimaudo, P. Moreno-Garcia, A. Riedo, M. B. Neuland, M. Tulej, P. Broekmann and P. Wurz, *Anal. Chem.*, 2015, **87**, 2037–2041.
- 18 I. Kuznetsov, J. Filevich, F. Dong, M. Woolston, W. L. Chao, E. H. Anderson, E. R. Bernstein, D. C. Crick, J. J. Rocca and C. S. Menoni, *Nat. Commun.*, 2015, **6**, 6944.
- 19 Y. Cui, J. F. Moore, S. Milasinovic, Y. M. Liu, R. J. Gordon and L. Hanley, *Rev. Sci. Instrum.*, 2012, **83**, 093702.
- 20 A. Riedo, A. Bieler, M. Neuland, M. Tulej and P. Wurz, *J. Mass Spectrom.*, 2013, **48**, 1–15.
- 21 P. Wurz, D. Abplanalp, M. Tulej and H. Lammer, *Planet. Space Sci.*, 2012, **74**, 264–269.
- 22 D. T. Snyder, C. J. Pulliam, Z. Ouyang and R. G. Cooks, *Anal. Chem.*, 2016, **88**, 2–29.
- 23 A. Riedo, A. Bieler, M. Neuland, M. Tulej and P. Wurz, *J. Mass Spectrom.*, 2013, **48**, 1–15.
- 24 A. Neubeck, M. Tulej, M. Ivarsson, C. Broman, A. Riedo, S. McMahon, P. Wurz and S. Bengtson, *Int. J. Astrobiol.*, 2016, **15**, 133–146.
- 25 A. Riedo, M. Tulej, U. Rohner and P. Wurz, *Rev. Sci. Instrum.*, 2017, **88**, 045114.
- 26 M. Tulej, S. Meyer, M. Luthi, D. Lasi, A. Galli, L. Desorgher, W. Hajdas, S. Karlsson, L. Kalla and P. Wurz, *Rev. Sci. Instrum.*, 2015, **86**, 083310.
- 27 H. Electronics, MCP Assembly, K. K. E. T. Division, 2006.
- 28 M. Hohl, P. Wurz, S. Scherer, K. Altwegg and H. Balsiger, *Int. J. Mass Spectrom.*, 1999, **188**, 189–197.
- 29 F. S. Anderson, J. Levine and T. J. Whitaker, *Rapid Commun. Mass Spectrom.*, 2015, **29**, 191–204.
- 30 A. Riedo, U. Rohner and P. Wurz, *Rev. Sci. Instrum.*, 2017, 045114.
- 31 A. Bieler, K. Altwegg, L. Hofer, A. Jackel, A. Riedo, T. Semon, P. Wahlstrom and P. Wurz, *J. Mass Spectrom.*, 2011, **46**, 1143–1151.
- 32 Behlke, FSWP 90 01 RS Datasheet.
- 33 X. H. Wang, S. D. Zhang, X. L. Cheng, E. Y. Zhu, W. Hang and B. L. Huang, *Spectrochim. Acta, Part B*, 2014, **99**, 101–114.
- 34 S. Meyer, M. B. Neuland, M. Tulej and P. Wurz, *J. Mass Spectrom.*, 2017, **52**(9), 580–590.
- 35 J. S. Becker, *Inorganic Mass Spectrometry*, John Wiley & Sons Ltd., 2007.
- 36 A. Al-Kathiri, E. Gnos and B. A. Hofmann, *Meteorit. Planet. Sci.*, 2007, **42**, 2137–2152.
- 37 D. Y. Liu, B. L. Jolliff, R. A. Zeigler, R. L. Korotev, Y. S. Wan, H. Q. Xie, Y. H. Zhang, C. Y. Dong and W. Wang, *Earth Planet. Sci. Lett.*, 2012, **319**, 277–286.
- 38 R. Tartese, M. Anand, K. H. Joy and I. A. Franchi, *Meteorit. Planet. Sci.*, 2014, **49**, A392.
- 39 E. Gnos, B. A. Hofmann, A. Al-Kathiri, S. Lorenzetti, O. Eugster, M. J. Whitehouse, I. M. Villa, A. J. Jull, J. Eikenberg, B. Spettel, U. Krahenbuhl, I. A. Franchi and R. C. Greenwood, *Science*, 2004, **305**, 657–659.